PERGAMON

International Journal of Multiphase Flow 28 (2002) 1737–1761

International Journal of Multiphase Flow

www.elsevier.com/locate/ijmulflow

Air–water flows down stepped chutes: turbulence and flow structure observations

H. Chanson *, L. Toombes

Department of Civil Engineering, The University of Queensland, Brisbane, Qld 4072, Australia

Received 26 August 2001; received in revised form 1 August 2002

Abstract

Interactions between turbulent waters and atmosphere may lead to strong air–water mixing. This experimental study is focused on the flow down a staircase channel characterised by very strong flow aeration and turbulence. Interfacial aeration is characterised by strong air–water mixing extending down to the invert. The size of entrained bubbles and droplets extends over several orders of magnitude, and a significant number of bubble/droplet clusters was observed. Velocity and turbulence intensity measurements suggest high levels of turbulence across the entire air–water flow. The increase in turbulence levels, compared to single-phase flow situations, is proportional to the number of entrained particles.

Keywords: Air–water flows; Stepped cascade; Turbulence; Bubbles; Droplets; Cluster; Experimental data

1. Introduction

Interactions between cascading water and atmosphere may lead to strong air–water mixing and complex multiphase flow situations. Air–water flows have been studied only recently. The first successful experiments were those of R. Ehrenberger in Austria and later the works led by L.G. Straub in North-America (Chanson, 1997a, pp. 15–16). Since the 1960s, numerous researchers studied gas entrainment in liquid flows although most studies focused on low void fractions ($C < 5\%$). Few research projects have been engaged in strongly turbulent flows associated with strong free-surface aeration (reviews by Wood, 1991; Chanson, 1997a).

* Corresponding author. Fax: +61-733-654-599.
E-mail address: h.chanson@mailbox.uq.edu.au (H. Chanson).
URL: http://www.uq.edu.au/~e2hchans.

0301-9322/02/$ - see front matter
PII: S0301-9322(02)00089-7

It is the aim of this work to gain some understanding of highly turbulent free-surface flows. The study examines cascading waters down a stepped chute. Up to date, detailed air–water studies of cascading flows have been limited (Table 1). New experimental investigations were conducted in a large-size facility where the flow was characterised by very energetic turbulence and free-surface aeration. The results illustrate complex interactions between turbulence and interfacial aeration.

1.1. Bibliographic review

In open channel flows, free-surface aeration is caused by a combination of wave instabilities and turbulence fluctuations acting next to the air–water free-surface (Keulegan and Patterson, 1940; Ervine and Falvey, 1987). Through this interface, there are continuous exchanges of both mass and momentum between water and atmosphere. Experimental evidence demonstrates that the air–water flow behaves as a homogeneous mixture for $C < 90\%$ where C is the void fraction (Cain, 1978; Wood, 1991; Chanson, 1997a). The mixture consists of water surrounding air bubbles (bubbly flow, $C < 30\%$), air surrounding water droplets (spray, $C > 70\%$) and an intermediate flow structure for $0.3 < C < 0.7$ (Fig. 1).

In turbulent water flows, air bubbles may be entrained when the turbulent kinetic energy is large enough to overcome both surface tension and gravity effects, which yields $v' > 0.1$–0.3 m/s where v' is an instantaneous turbulent velocity normal to the flow direction (Ervine and Falvey, 1987; Chanson, 1993). The condition is nearly always achieved in stepped chute flows because of the very energetic turbulence generated by the stepped invert (Fig. 1). Considering a given stepped geometry, low flow rates give rise to a succession of free-falling nappes called nappe flow regime, and relatively little aeration is observed (Chamani and Rajaratnam, 1994; Chanson, 1994). With increasing flow rates, a transition flow regime occurs at intermediate discharges. Dominant flow features included a chaotic appearance and strong splashing associated with irregular droplet ejections that are seen to reach heights of up to 3–5 times the step height (Chanson, 2001). At larger flow rates, the waters skim over the pseudo-bottom formed by the step edges (skimming flow regime). Intense cavity recirculation is observed and the flow resistance is form drag predominantly (Rajaratnam, 1990; Chanson, 1995).

In both transition and skimming flows, the upstream flow is non-aerated as sketched in Fig. 1A, but free-surface instabilities are observed. The location of the inception of free-surface aeration is clearly defined. Downstream the flow becomes rapidly aerated and free-surface aeration is very intense (Fig. 1).

2. Experimental apparatus

New experiments were conducted at the University of Queensland in a 5-m long, 1-m wide test section (Fig. 1, Table 1). Water was supplied from a large feeding basin (1.5-m deep, surface area 6.8 m $\times$ 4.8 m) leading to a sidewall convergent with a 4.8:1 contraction ratio. The intake geometry yielded low inflow turbulence. Two stepped slopes were tested. One test section consisted of a 0.9-m high, 0.88-m long broad-crested weir with upstream rounded corner (0.057-m radius), followed by nine identical steps ($h = 0.1$ m, $l = 0.35$ m) made of marine ply. The second geometry consisted of a broad-crested weir (0.6-m long) followed by nine identical steps ($h = 0.1$ m,

Table 1
Detailed experimental investigations of air entrainment in stepped chutes

Reference (1)	α (deg) (2)	q_w (m^2/s) (3)	h (m) (4)	Flow regime (5)	Instrumentation (6)	Remarks (7)
Chanson and Toombes (1997, 2000)	3.4	0.038–0.163	0.143	Nappe flow	Single-tip conductivity probe ($\varnothing = 0.35$ mm)	$L = 24$ m. $W = 0.5$ m. Supercritical inflow (0.03-m nozzle thickness)
Tozzi et al. (1998)	52.2	0.23	0.053	Skimming flow	Conductivity probe	Inflow: uncontrolled smooth WES ogee crest followed by smaller first steps
Chamani and Rajaratnam (1999)	51.3 and 59	0.07–0.2	0.313–0.125	Skimming flow	Conductivity probe and flushed Pitot tube ($\varnothing = 3.2$ mm)	$W = 0.30$ m. Inflow: un-controlled smooth WES ogee crest
Matos (2000)	53.1	0.08–0.2	0.08	Skimming flow	Conductivity probe flushed Pitot tube ($\varnothing = 3.2$ mm)	$W = 1$ m. Inflow: uncontrolled WES ogee crest, with small first steps built in the ogee development
Toombes and Chanson (2000)	3.4	0.08–0.136	0.143	Nappe flow	Double-tip conductivity probe ($\varnothing = 0.025$ mm)	$L = 3.2$ m. $W = 0.25$ m. Supercritical inflow (nozzle thickness: 0.028–0.040 m). Ventilated steps
Boes (2000)	30 and 50	0.047–0.38	0.023–0.09	Skimming flow	Double-tip optical fibre probe RBI ($\varnothing = 0.1$, 2.1 mm spacing between sensors)	$W = 0.5$ m. Inflow: pressurised intake
Ohtsu et al. (2000)	55	0.016–0.03	0.025	Skimming flow	Single-tip optical fibre probe	$W = 0.3$ m. Inflow: uncontrolled broad crest
Present study	21.8	0.04–0.18	0.1	Transition and Skimming flows	Double-tip conductivity probe ($\varnothing = 0.025$ mm)	$L = 3.0$ m. $W = 1$ m. Inflow: uncontrolled broad crest. Experiments TC200
	15.9	0.05–0.26	0.1	Transition and Skimming flows	Double-tip conductivity probe ($\varnothing = 0.025$ mm)	$L = 4.2$ m. $W = 1$ m. Inflow: uncontrolled broad crest. Experiments TC201

Notes: L: chute length; W: chute width.

$l = 0.25$ m) made of marine ply. The stepped chute was 1-m wide with perspex sidewalls, followed by a horizontal concrete-invert canal ending in a dissipation pit. The flow rate was delivered by a

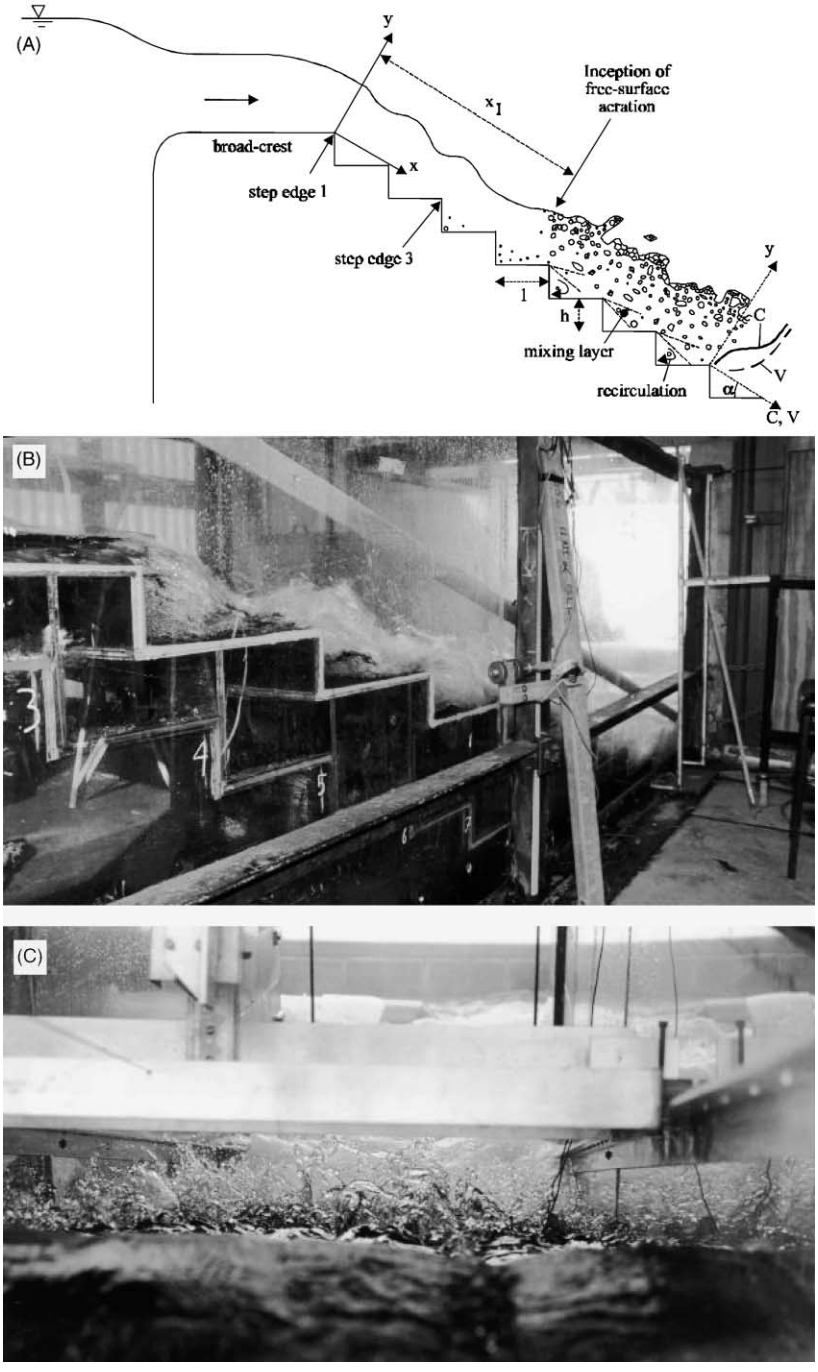

Fig. 1. Sketch and photograph of stepped chute flows: (A) Definition sketch. (B) $\alpha = 16°$, $h = 0.1$ m, $q_w = 0.070$ m^2/s, transition flow regime—flow from the top left to the bottom right. Note the 22° stepped invert visible beneath the 16° cascade. (C) Details of the spray region in skimming flow ($\alpha = 16°$, $h = 0.1$ m, $q_w = 0.186$ m^2/s)—flow from the foreground to the background.

pump controlled with an adjustable frequency AC motor drive, allowing an accurate discharge adjustment in a closed-circuit system. Further details on the experimental facilities may be found in Chanson and Toombes (2001).

2.1. Instrumentation

The discharge was measured from the upstream head above crest with an accuracy of about 2% (Ackers et al., 1978; Bos, 1976). Clear-water flow depths and velocities were measured with a point gauge and a Prandtl–Pitot tube ($\varnothing = 3.3$ mm) respectively. Air–water flow properties were measured using a double-tip conductivity probe ($\varnothing = 0.025$, 7.775 mm spacing between sensors). The probe sensors were aligned in the flow direction (Fig. 2A and B) and excited by an air bubble detector (AS25240). The probe signal was scanned at 20 kHz per sensor for 20–40 s. Initial experiments were conducted with a single-tip conductivity probe ($\varnothing = 0.35$ mm) with sampling times ranging from 60 to 180 s. For identical flow conditions, comparative results showed no difference in void fraction distributions between dual-tip and single-tip probe data.

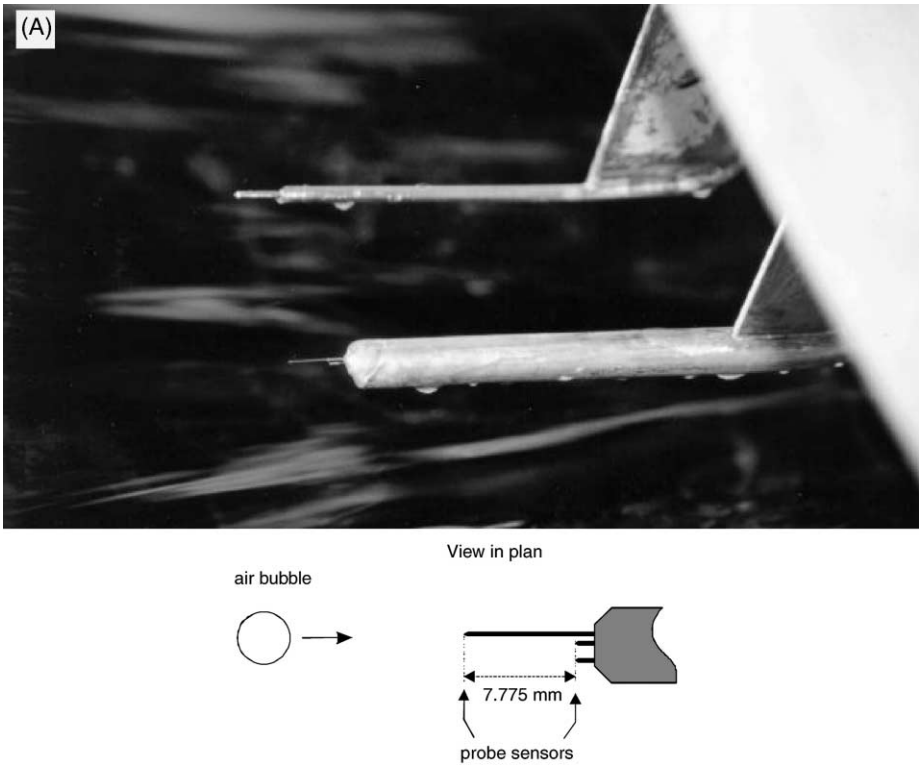

Fig. 2. Details of the double-tip resistivity probe characteristics: (A) Photograph of the single-tip (top left) and double-tip (bottom right) probes above water, flow from the left to the right. (B) Sketch of the dual-tip conductivity probe. (C) Normalised auto- and cross-correlation functions for $\alpha = 15.9°$, $h = 0.1$ m, $d_c/h = 1.53$, skimming flow, step edge 8: $(x - x_I)/d_c = 5.93$, $C_{mean} = 0.31$, $Y_{90}/d_c = 0.56$, $V_{90}/V_c = 2.82$, $F_{max}d_c/V_c = 29.4$.

(B)

Ref.	y/d_c	C	$F\ d_c/V_c$	V/V_c	Tu
St8_04	0.163	0.065	12.3	2.26	0.30
St8_09	0.391	0.505	28.4	2.76	1.79
St8_11	0.482	0.806	17.6	2.82	0.63

(C)

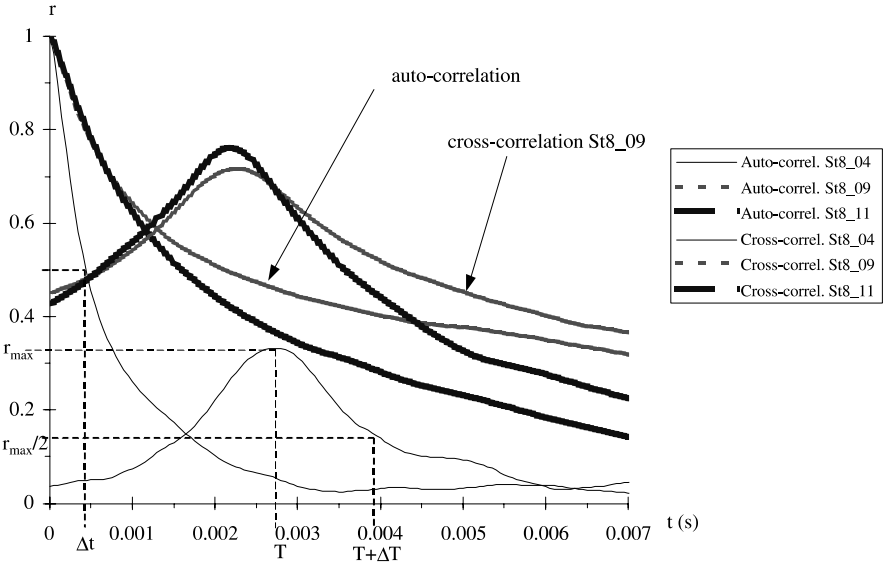

Fig. 2 (*continued*)

The translation of the probes in the direction y normal to the pseudo-invert formed by the step edges was controlled by a fine adjustment travelling mechanism connected to a Mitutoyo™ digimatic scale unit. The error on the normal position of the probe was less than $\Delta y < \pm 0.025$ mm. The accuracy on the longitudinal position of the probe was estimated as $\Delta x < \pm 0.5$ cm. The accuracy on the transverse position of the probe was less than 1 mm. Flow visualisations were conducted with a digital video-camera Sony™ DV-CCD DCR-TRV900 (shutter: 1/4 to 1/10,000 s) and high-speed still photographs (shutter: 1/2000 s) (Fig. 1B).

2.2. Data processing

Air–water flow properties were recorded for transition flows (i.e. $0.5–0.7 < d_c/h < 1.1–1.3$) and skimming flows (i.e. $d_c/h > 1.1–1.3$), where d_c is the critical flow depth and h is the vertical step height. In rectangular channels, $d_c = (q_w^2/g)^{1/3}$ where q_w is the water discharge per unit width and g is the gravity acceleration. Void fractions, bubble count rates and chord times were calculated from the probe leading tip signal using a single-threshold technique. The threshold was set at 50% and checked to remain at $50 \pm 5\%$ of the probe voltage range, despite air and water voltage level fluctuations during a scan period.

Velocities were calculated using a cross-correlation technique (e.g. Crowe et al., 1998). The dimensionless turbulent velocity fluctuations were estimated from the broadening of cross-correlation function compared to auto-correlation function:

$$\mathrm{Tu} = \frac{u'}{V} = 0.851\frac{\sqrt{\Delta T^2 - \Delta t^2}}{T} \quad (1)$$

where u' is the root mean square of longitudinal component of turbulent velocity, V is the local, time-averaged air–water velocity, ΔT is the time scale satisfying: $r(T + \Delta T) = r_{max}/2$, r is the cross-correlation coefficient function and r_{max} is the maximum cross-correlation, Δt is the characteristic time for which the auto-correlation function equals 0.5, and T is the bubble travel time for which the cross-correlation function is maximum (i.e. $r(T) = r_{max}$). Eq. (1) is based upon an extension of the mean value theorem for definite integrals (Appendix A). Fig. 2C presents three series of correlation data taken at the same cross-section, for identical flow conditions and at different elevations.

3. Void fraction and bubble count rate distributions

Downstream of the inception point of free-surface aeration, air and water were fully mixed, forming a homogeneous two-phase flow (Chanson, 1997a, 2001). The advective diffusion of air bubbles may be described by simple analytical models: that is, Eqs. (2) and (3) developed by Chanson and Toombes (2001) based upon the reasoning of Chanson (1997a).

In the low range of transition flows (i.e. $0.5–0.7 < d_c/h < 0.75–0.9$), the flow was highly aerated at each and every cross-section, with depth-average mean air concentrations ranging from 40% to 75%. At step edges, the distributions of void fraction followed closely:

$$C = K'\left(1 - \exp\left(-\lambda\frac{y}{Y_{90}}\right)\right) \quad (2)$$

where y is distance measured normal to the pseudo-invert (Fig. 1A), Y_{90} is the characteristic distance where $C = 90\%$, K' and λ are dimensionless functions of the mean air content only (Appendix B). Eq. (2) compares favourably with experimental data (Fig. 3A). In Fig. 3A, Eq. (2) is plotted for only one value of mean air content.

In the upper range of transition flows and in skimming flows (i.e. $d_c/h > 0.75–0.9$), the air concentration profiles have a smooth, continuous shape which may be modelled by

$$C = 1 - \tanh^2\left(K'' - \frac{\frac{y}{Y_{90}}}{2D_o} + \frac{\left(\frac{y}{Y_{90}} - \frac{1}{3}\right)^3}{3D_o}\right) \quad (3)$$

where K'' is an integration constant and D_o is a function of the mean void fraction only (Appendix B). Data at both step edges and half-distance between step edges are compared successfully with Eq. (3) in Fig. 3B. Note that, in Fig. 3B, Eq. (3) is plotted for only two values of mean air content.

The results showed further a marked change between void fraction distributions measured at step edges and above the recirculating cavities (Fig. 3A and B). Greater flow aeration was observed consistently between step edges (Fig. 3A (symbols $*$) and B (symbols $+$, $\times$, $*$)) than at the adjacent step edges. This effect was particularly marked in the fluid layers next to the recirculation cavity (i.e. $y/Y_{90} < 0.3–0.4$). Similar observations were reported by Boes (2000) and Matos et al. (2001). It is believed that cavity aeration is enhanced by inertial forces acting on air bubbles

(A)

Ref.	d_c/h	$(x-x_I)/d_c$	C_{mean}	Y_{90}/d_c	V_{max}/V_c	$F_{max}d_c/V_c$	Location
Q22_S4	0.70	4.81	0.63	0.85	2.89	10.4	step edge
Q22_S5	0.70	8.65	0.56	0.78	3.29	13.7	step edge
Q22_S7	0.70	16.35	0.55	0.79	3.61	19.6	step edge
Q22_S8	0.70	20.19	0.52	0.66	3.13	21.1	step edge
Q32_S5	0.78	6.97	0.48	0.69	2.91	16.0	step edge
Q32_S6	0.78	11.62	0.45	0.73	2.86	18.3	step edge
Q32_S7	0.78	16.26	0.48	0.68	3.06	19.0	step edge
Q32_S8	0.78	20.91	0.48	0.80	2.91	18.6	step edge
Q32_S7A	0.78	18.59	0.77 (?)	0.74	2.86	12.4	1/2 between edges

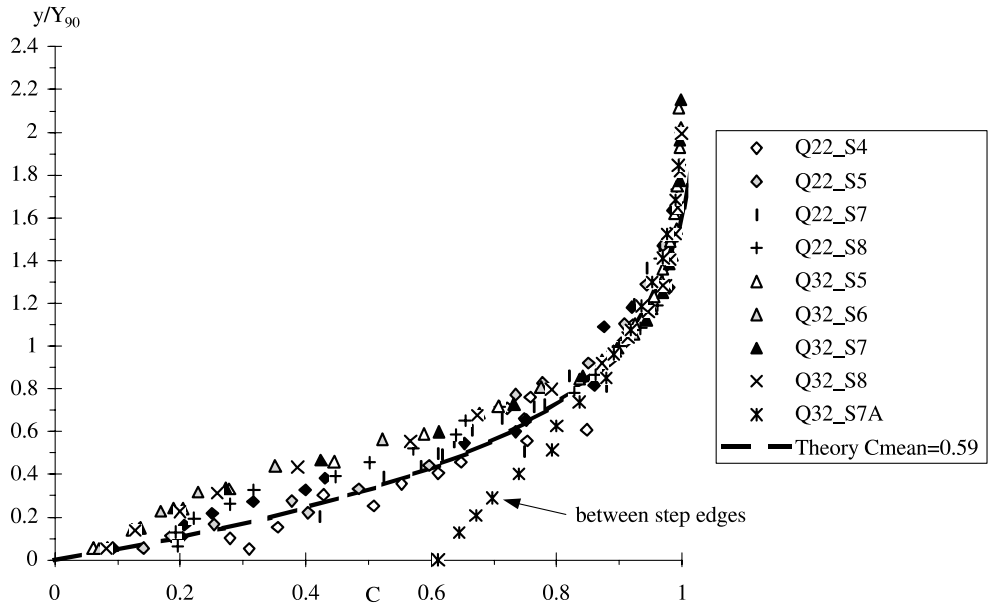

Fig. 3. Dimensionless void fraction distributions: (A) Transition flows ($h = 0.1$ m): data measured at outer step edges and at half-distance between edges. (B) Skimming flows ($h = 0.1$ m): data measured at step edges and at half-distance between step edges.

trapped in the core of recirculating vortices (e.g. Tooby et al., 1977). Vortex trapping of bubbles leads to higher air content in the cavity flow and in the mixing layers downstream of the step edges (Fig. 1).

3.1. Bubble count rates

Fig. 4 presents dimensionless distributions of bubble count rates $F\ d_c/V_c$, where V_c is the critical flow velocity. In rectangular channels, $V_c = (gd_c)^{1/2}$. The data are compared with a parabolic curve:

(B)

Ref.	d_c/h	$(x-x_I)/d_c$	C_{mean}	Y_{90}/d_c	V_{90}/V_c	$F_{max}d_c/V_c$	Location
Q23_S6	1.50	0.45	0.23	0.51	2.63	7.7	step edge
Q23_S7	1.50	2.24	0.23	0.47	2.79	13.6	step edge
Q23_S8	1.50	4.04	0.38	0.59	2.85	16.4	step edge
Q21_S7	1.10	5.51	0.43	0.59	3.00	27.4	step edge
Q21_S8	1.10	7.96	0.43	0.54	2.99	29.9	step edge
Q31_S7	1.53	3.56	0.34	0.55	2.76	23.3	step edge
Q31_S8	1.53	5.93	0.31	0.56	2.82	29.4	step edge
Q21_S7A	1.10	6.73	0.53	0.64	2.88	21.7	1/2 between edges
Q31_S7A	1.53	4.74	0.48	0.62	2.75	20.9	1/2 between edges
Q31_S8A	1.53	7.12	0.46	0.65	2.76	23.8	1/2 between edges

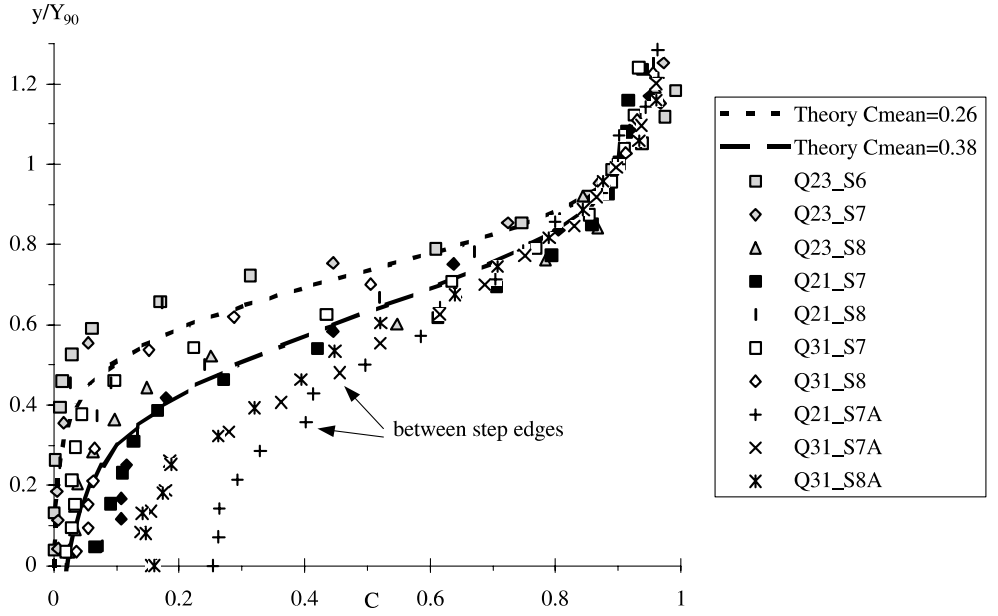

Fig. 3 (*continued*)

$$\frac{F}{F_{max}} = 4C(1-C) \tag{4}$$

where F_{max} is the maximum bubble frequency observed for $C = 50\%$. In Fig. 4A and B, only one parabolic curve is shown for comparison. Such a parabolic relationship was previously observed in open channel flows, hydraulic jumps and plunging jet flows (e.g. Chanson, 1997b; Chanson and Brattberg, 2000). Toombes (2002) demonstrated the unicity of the relationship between bubble frequency and void fraction, and he derived Eq. (4) for an air–water structure with constant, equal minimum bubble and droplet sizes in a cross-section.

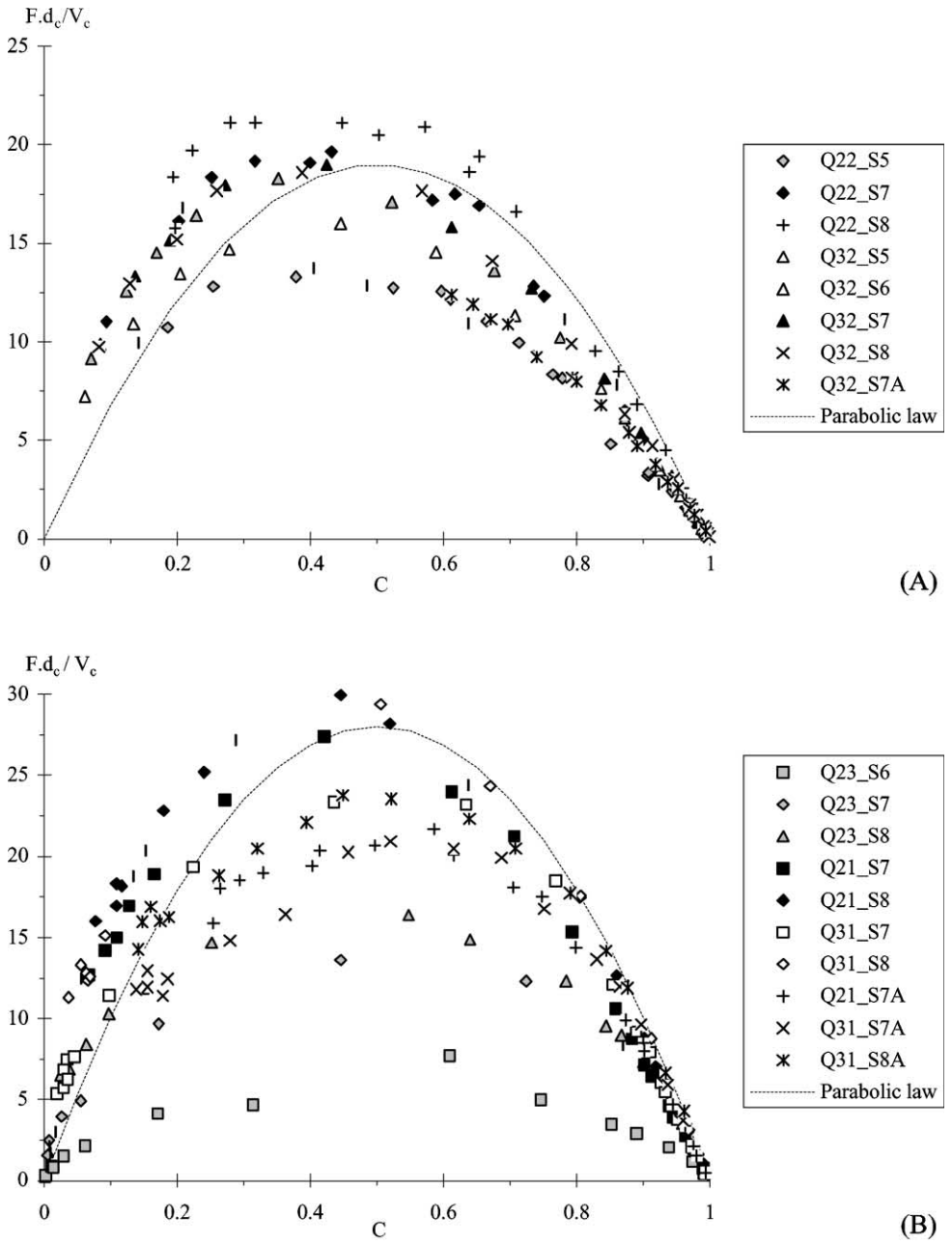

Fig. 4. Dimensionless bubble count rate distributions (flow characteristics are detailed in Fig. 3): (A) transition flows, (B) skimming flows.

Measurements conducted at half-distance between step edges, in transition and skimming flows, showed that, for $y/h \leqslant 0.1$, bubble count rates data were larger by about 10–20% than at a higher location (i.e. $y/h > 0.1$) for an identical void fraction. It is believed that large shear stresses

in the mixing layer induced some additional bubble breakup, which in turn enlarged the count rate for the same void fraction.

4. Air–water velocity and velocity fluctuation profiles

Air–water velocity distributions are presented in Figs. 5 and 6 in terms of the time-averaged air–water velocity V and turbulence intensity Tu respectively.

In transition flows, the velocity measurements show quasi-uniform velocity profiles at step edges (Fig. 5A). Overall the data at step edges were correlated by

$$\frac{V}{V_{max}} \sim 0.85 + 0.075\left(\frac{y}{Y_{90}}\right) \quad \text{for } y/Y_{90} < 2 \tag{5}$$

where V_{max} is the maximum velocity, usually observed at about $y/Y_{90} = 1.6$–2. Eq. (5) is shown in Fig. 5A. It has no theoretical justification and it is only a rough correlation. Transition flows are characterised by relatively small water depth compared to the step roughness height: i.e., $d/(h\cos\alpha) < 0.4$ typically where d is the equivalent clear-water depth and α is the slope of the pseudo-bottom formed by the step edge (Fig. 1). It is hypothesised that large energy dissipation taking place at each step is associated with very energetic turbulent mixing across the entire air–water flow. In turn the strong momentum mixing yields quasi-uniform velocity profiles.

In skimming flows, velocity data measured at step edges compare favourably with a power law:

$$\frac{V}{V_{90}} = \left(\frac{y}{Y_{90}}\right)^{1/6} \tag{6}$$

where V_{90} is the characteristic velocity at $y = Y_{90}$ (Fig. 5B). The result is close to that of Matos (2000) and Boes (2000). Boes (2000) observed a power law exponent of 1/6.7 for $\alpha = 30°$ and 1/5.8 for $\alpha = 50°$. Matos obtained a 1/5.1 power law but he used a flushed Pitot tube (Table 1, column 7), and the different type of instrumentation might explain some difference.

The velocity distribution results in skimming flows are basically identical to measured velocity distributions in self-aerated flows on smooth-invert chutes (Cain, 1978; Chanson, 1997a,b), although the rate of energy dissipation is much greater on a stepped cascade and flow resistance is dominated by form drag. Between step edges, the mixing layers interact with the free-stream. At half-distance between step edges, measurements showed that $V(y = 0) = 0.75V_{90}$ in average, independently of the step geometry and flow rate (Fig. 5B).

4.1. Turbulent velocity fluctuations

Fig. 6 presents distributions of turbulence intensity $Tu = u'/V$ where Tu is a dimensionless measure of the turbulent fluctuations of interfacial velocity. The results exhibit relatively high turbulence levels across the entire air–water flow mixture (i.e. $0 \leqslant y \leqslant Y_{90}$) (Fig. 6). The trend, observed in both skimming and transition flows, differs significantly from well-known turbulence intensity profiles observed in turbulent boundary layers (e.g. Schlichting, 1979). It is believed that the high rate of energy dissipation, associated with form drag generated by the steps, contributes

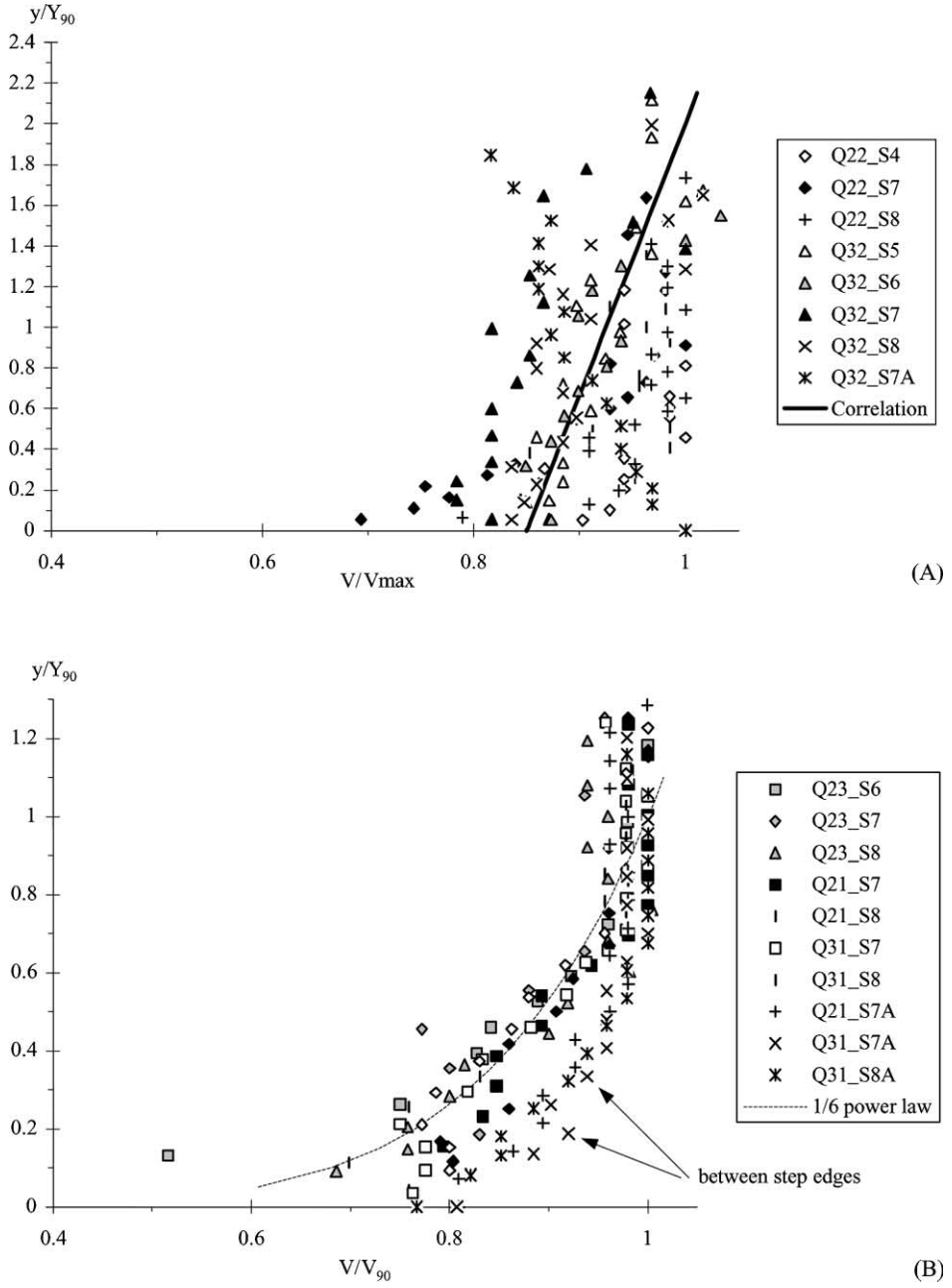

Fig. 5. Dimensionless air–water velocity distributions (flow characteristics are detailed in Fig. 3): (A) Transition flows: comparison between data and Eq. (5). (B) Skimming flows: comparison between data and Eq. (6).

to strong turbulent mixing throughout the entire flow. Although the quantitative values of turbulence intensity are large (Tu $\sim$ 100%), they are similar to turbulence measurements in separated flows past rectangular cavity (Haugen and Dhanak, 1966), in wakes between large stones

Ref.	d_c/h	$(x-x_I)/d_c$	C_{mean}	Y_{90}/d_c	V_{90}/V_c	$F_{max}d_c/V_c$	Location
Q23_S7	1.50	2.24	0.23	0.47	2.79	13.6	step edge
Q23_S8	1.50	4.04	0.38	0.59	2.85	16.4	step edge
Q31_S8	1.53	5.93	0.31	0.56	2.82	29.4	step edge
Q23_S7A	1.50	3.14	0.40	0.60	2.73	15.2	1/2 between edges
Ohtsu & Yasuda (1997)	1.86	-1.65	0	$d/d_c = 0.43$	$V_{max}/V_c = 3.42$	0	step edge upstream inception pt

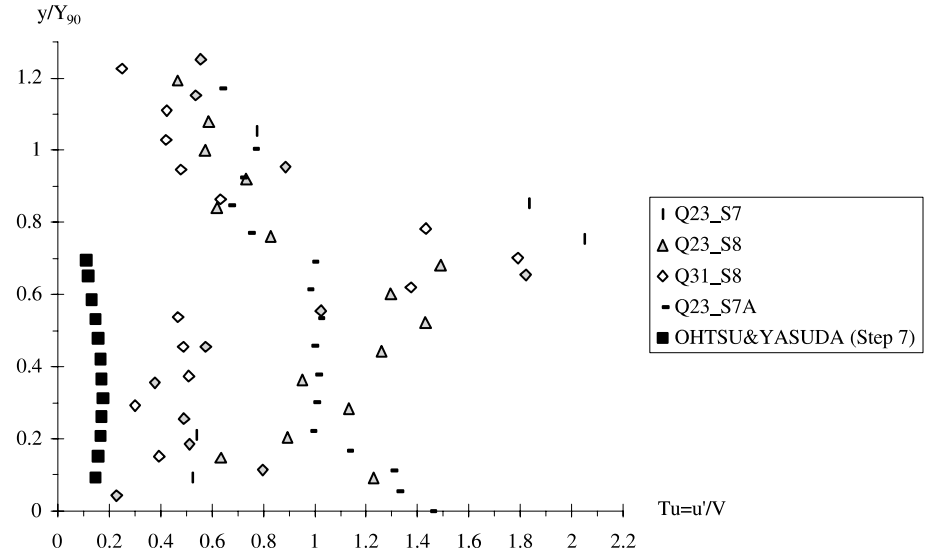

Fig. 6. Turbulent intensity distributions in skimming flows.

(Sumer et al., 2001), in developing shear region of plunging water jets (Chanson and Brattberg, 1998) and in pipe flows (Mudde and Saito, 2001). Note that only the metrology of Mudde and Saito was comparable to the present signal processing technique. Other studies recorded the turbulent velocity fluctuations in the water phase using hot film probes and LDV.

In Fig. 6, skimming flow data are compared with monophase flow LDV measurements by Ohtsu and Yasuda (1997) performed in skimming flow down a 19° stepped chute ($h = 0.05$ m), immediately upstream of the inception point of free-surface aeration. Their data exhibit a profile significantly different from turbulent boundary layer flows (e.g. Schlichting, 1979) and relatively close to the present results. The difference between Ohtsu and Yasuda's results and present observations suggests a drastic increase in turbulence level associated with air bubble entrainment. Deviations between monophase flow data and air–water flow data take place for void fractions ranging from 0.05 to 0.95 with maximum turbulence intensity observed for $C = 0.4$–0.6 for all experiments in transition and skimming flows. It is believed that the increase in turbulence level is directly linked to the number of entrained bubbles/droplets. Fig. 7 presents turbulence intensity data as a function of the dimensionless bubble count rate. The turbulence data are correlated to the dimensionless bubble frequency by

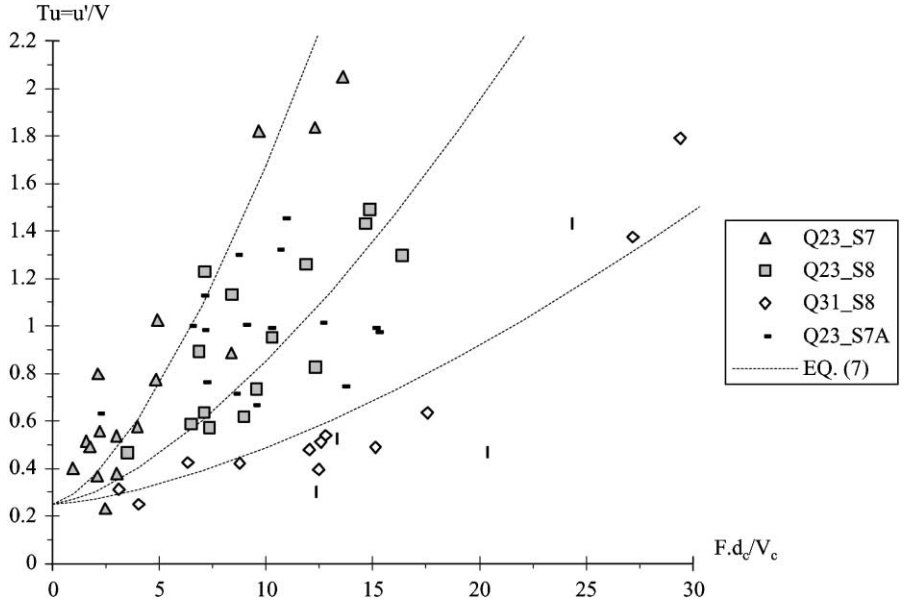

Fig. 7. Relationship between turbulent intensity and dimensionless bubble count rate in skimming flows (flow characteristics are detailed in Fig. 6).

$$\mathrm{Tu} = 0.25 + k\left(\frac{Fd_c}{V_c}\right)^{1.5} \tag{7}$$

where k is a constant of proportionality which is a function of the step geometry and location, and flow rate. Eq. (7) was observed in both transition and skimming flows, at step edge and between step edges. It reflects an increase in turbulence associated with the number of entrained particles. For low bubble count rates (i.e. $Fd_c/V_c < 2$), the result (Eq. (7) and Fig. 7) yields $\mathrm{Tu} \approx 0.25$ which is close to the observations of Ohtsu and Yasuda (1997) in single-phase skimming flows (Fig. 6).

4.2. Discussion

The results show turbulence levels in air–water flows of about one order of magnitude greater than monophase flow data. A similar observation was made in pipe flows: e.g., Wang et al. (1990), Lance and Bataille (1991), Mudde and Saito (2001) for low void fractions; Liu and Bankoff (1993) for $C < 0.5$. However two differences must be noted. First, in the present study, the flow velocity was 10–20 times greater than the bubble rise velocity of observed millimetric bubbles. Second the quantitative levels of bubble-induced turbulence were greater than observations in pipe flows. Mudde and Saito (2001) suggested that bubble-induced turbulence might result from a combination of shear, potential flow around a bubble, wake and "vortical structures caused by non-uniform distribution of bubbles". Their estimate of the contribution of the first three effects yield $\mathrm{Tu} \sim 22\%$ for $C = 0.5$ and $V = 3$ m/s assuming a bubble rise velocity of 0.25 m/s (e.g. Comolet, 1979). While the contribution of vortical structures is certainly significant, the drastic increase in

turbulent velocity fluctuations observed in Fig. 6 must be attributed to other factors, including particle collisions, breakup and coalescence which all affect the interfacial velocity field.

5. Bubble/droplet size distributions and clustering

5.1. Bubble/droplet size distributions

Bubble and droplet chord length measurements, performed on both transition and skimming flows, show a broad spectrum of bubble/droplet chord lengths at each location extending over several orders of magnitude. During the study, the minimum size of bubbles resolvable by the probe was about 0.1 mm.

The chord length distributions are typically skewed with a preponderance of small bubble/droplet sizes relative to the mean (e.g. Fig. 8A). Fig. 8A presents normalised probability distribution functions of bubble sizes in the bubbly flow region ($C < 0.3$), all data being recorded at the same cross-section for the same flow rate. Although the probability of air bubble chord lengths is the largest for bubble sizes between 0 and 2 mm, it is worth noting some amount of bubbles larger than 20 mm (Fig. 8A, last column >20). The probability distribution functions of bubble chord length tend to follow, on average, a log–normal distribution. Note that a gamma distribution provides also a good fit.

Water droplet chord length distributions are also skewed with a preponderance of small drop sizes relative to the mean. The droplet size distributions differ however from bubble chord length distributions. For the same void and liquid fraction, the droplet chord mode and mean are larger than the corresponding bubble chord length data (Fig. 8B). Fig. 8B shows mean chord sizes as function of the local void/liquid fractions. For $C = 0.5$, the mean droplet and bubble chord sizes are equal. For void/liquid fractions less than 0.2–0.3, the mean droplet chord length (Fig. 8B, black symbols) is consistently larger than the corresponding mean bubble size (Fig. 8B, white symbols). The result is most pronounced for void/liquid fractions less than 0.05.

5.2. Bubble clustering effect

The streamwise distribution of bubbles and droplets was analysed. A cluster of particles is defined as a group of two or more particles, with a distinct separation from other particles before and after the cluster. In a cluster, the particles are close together and the packet is surrounded by a sizeable volume of the other phase. (Note that the terms "packet", "cluster" and "platoon" are sometimes used for the same meaning.)

In bubbly flow (i.e. $C < 0.3$), two bubbles were considered to form a cluster when they were separated by a water chord length smaller than one-tenth of the mean water chord size. In skimming flows, 44% of air bubbles in average were associated with bubble clusters, almost independently of void fractions and mean chord length sizes. The average size of cluster bubbles was about 13% larger than the average bubble size. Nearly 68% of clusters were comprised of two bubbles (Fig. 9). In transition flows, 30% of the bubbles on average were grouped in clusters, while about 78% of the clusters were made of two bubbles. A similar analysis of droplet clusters was performed in the spray region (i.e. $C > 0.7$). Two droplets were assumed to form a packet if they

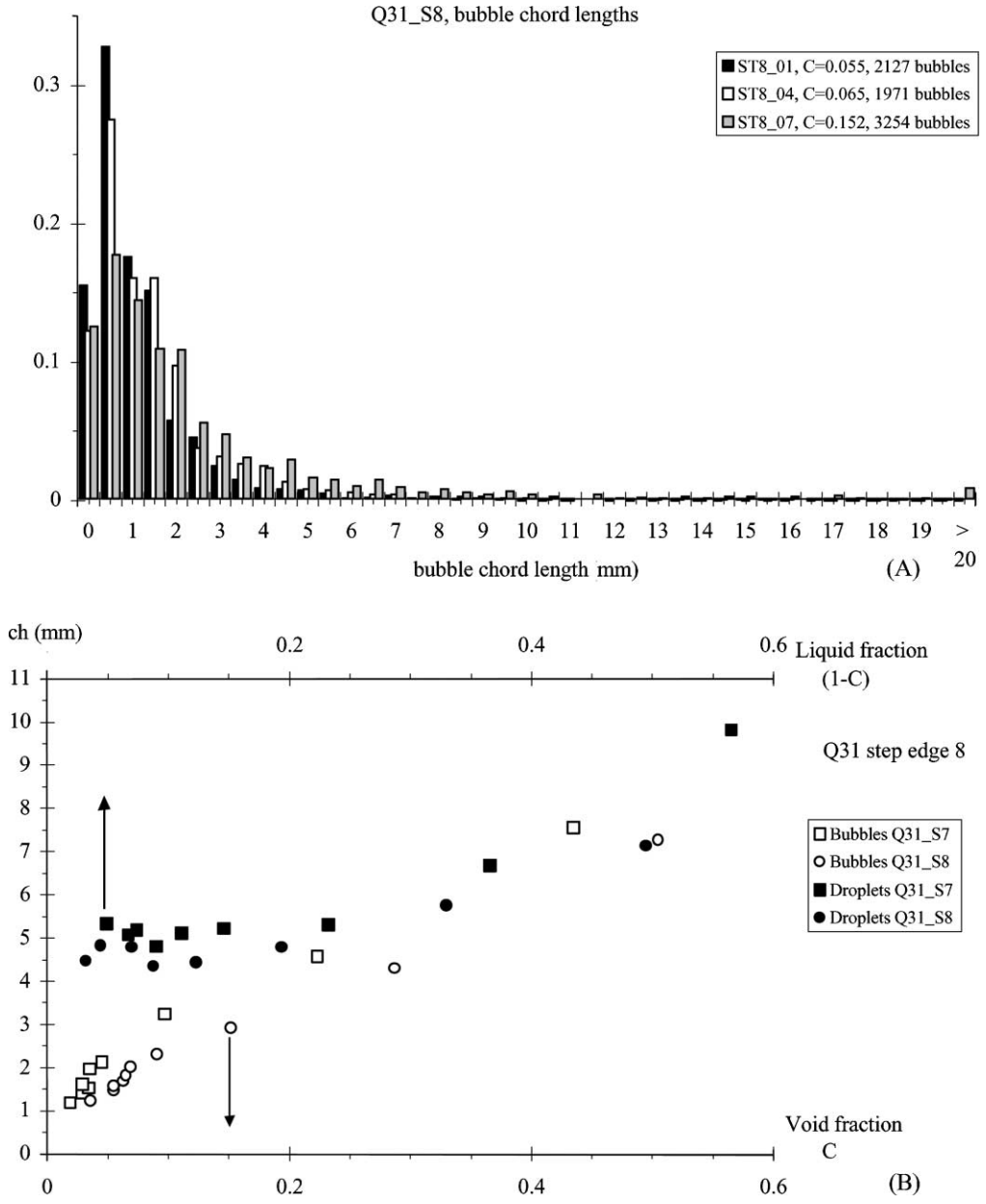

Fig. 8. Bubble and droplet chord length distributions (flow characteristics are detailed in Fig. 6): (A) Normalised probability distribution functions of bubble and droplet sizes in 0.5 mm intervals. (B) Distributions of mean bubble/droplet chord length as functions of the void/liquid fraction.

were separated by an air chord length smaller than one-tenth of the mean water chord size. In skimming flows, the results showed a slightly smaller number of droplet clusters: i.e., an average 41% of detected droplets formed a cluster, and about 73% of clusters included two droplets only. However the percentage of cluster droplets decreased from 70% down to 30% with increasing

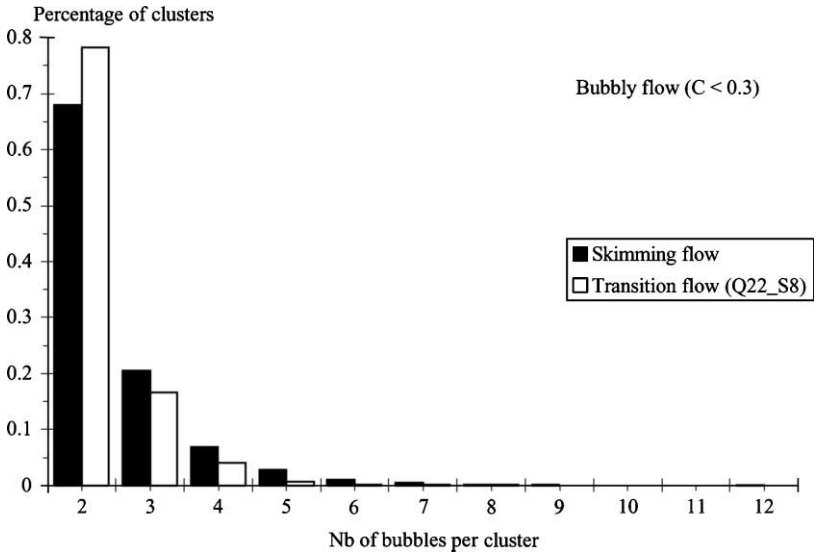

Fig. 9. Number of bubbles per cluster in bubbly flows ($C < 0.3$): Transition flows: 17,834 bubbles, 2364 clusters, skimming flows: 34,027 bubbles, 5607 clusters.

liquid fraction $(1 - C)$ from 0 to 0.3, while the percentage of two droplets clusters increased from 50% up to 80% with increasing liquid fractions.

Overall, the data demonstrated that a large proportion of particles (bubbles and droplets) travelled as part of a cluster structure, consisting typically of two particles only. For the same void and liquid fraction, the probability of a bubble travelling as part of a packet was about the probability of a droplet to travel in a cluster. The outcome was not expected, considering that water droplets have a momentum response time about 46,000 times larger than that of an air bubble of identical diameter (e.g. Crowe et al., 1998). The existence of bubble/droplet clusters may be related to breakup and coalescence, and to other processes. As the bubble response time is significantly smaller than the characteristic time of the flow, it is believed that bubble trapping in large-scale turbulent structures is a dominant clustering mechanism in the bubbly flow region. In the spray region, drop formation results from surface distortion, tip-streaming of ligaments and interactions between eddies and free-surface (e.g. Hoyt and Taylor, 1977; Rein, 1998) (Fig. 1C). The droplet ejection process is likely to be the dominant effect because the droplet response time is nearly two orders of magnitude larger the air flow response time.

5.3. Remarks

It must be emphasised that the present analysis is limited to cluster detection along a streamline. In particular, it does not consider bubble or droplets travelling side by side as being a cluster.

A sensitivity analysis was performed in bubbly flows ($C < 0.3$, skimming flows) to ascertain the representativity of the results. It was shown that the number of detected bubbles had to be greater than 600–800 for the cluster analysis results to be within 10% of the mean value, in terms of number of clusters, number of bubbles per cluster and size of bubbles in clusters. The cluster

analysis highlighted further the dual requirements to record a large number of bubble/droplet detections to improve the representativity of the samples, and to detect small water/air chord lengths associated with thin air–water interfaces. The writers believe that the present data acquisition rate (20 kHz per sensor for 20–40 s) was adequate in bubbly flows, but longer recording times would be suitable in the spray region.

Cummings and Chanson (1999) investigated air bubble entrainment at low-velocity plunging jet flows. They recorded the number of bubbles resulting from a single bubble breakup, and the size of both mother and daughter bubbles. For entrained bubble sizes less than 5.5 mm, most single breakups yielded two bubbles, forming a cluster without a preferential size significantly different from the mean. The results are close to the present observations although the flow configuration is significantly different.

6. Discussion

Skimming flows in stepped cascades exhibit some analogy with boundary layer flows past closely spaced cavities: i.e., d-type roughness (e.g. Djenidi et al., 1994, 1999). In both situations, irregular ejections of cavity fluid take place and the process appears to be sequential from upstream to downstream (Table 2). For example Elavarasan et al. (1995) and Djenidi et al. (1999) in boundary layer flows past rectangular cavities; Chanson et al. (2000) and Chanson and Toombes

Table 2
Observations of cavity ejections

Reference	Average ejection frequency ($F_{ej}k_s/V_o$)	Ejection duration ($k_s/V_o t_{burst}$)	Comments
(1)	(2)	(3)	(4)
Experimental observations			
Djenidi et al. (1994)	$0.182(k_s/\delta_{BL})$	(k_s/δ_{BL})	Water tunnel ($d = 0.26$ m, $W = 0.26$ m). $V_o = 0.4$ m/s, $\delta_{BL} = 0.035$ m, $\delta_M = 0.0025$ m. Square cavities: $k_s = 5$ mm
Tantirige et al. (1994)	0.017	0.138	Square tunnel ($d = 0.025$ m, $W = 0.025$ m). Fully developed inflow. $V_o = 0.43$ m/s. Triangular cavity: $k_s = 1.5$ mm, $\theta = 45°$
Lin and Rockwell (2001)	$0.53(V_o/k_s)$	–	Water tunnel ($d = 0.419$ m, $W = 0.547$ m). $V_o = 0.267$ m/s, $\delta_{BL} = 0.046$ m, $\delta* = 0.0069$ m, $\delta_M = 0.005$ m. Rectangular cavity: $k_s = 102$ mm, length up to 406 mm
Analytical calculations			
Chanson and Toombes (2001)	$f/5$	–	Skimming flow on stepped chute. Assuming all energy losses to take place by viscous dissipation in the cavity recirculation
Lin and Rockwell (2001)	$0.017(k_s/\delta_M)$	–	Linear stability theory for a convective-type instability

Notes: d: channel height; F_{ej}: average ejection frequency; f: Darcy friction factor; k_s: cavity depth; k_s': skin roughness height; l_{cav}: cavity length; V_o: free-stream velocity; δ_{BL}: boundary layer thickness; $\delta*$: displacement thickness; δ_M: momentum thickness; t_{burst}: ejection duration.

(2001) in skimming flows. Further the velocity profiles appear to be little affected by the cavity recirculation process. In skimming flows, the velocity profile follows a 1/6th power law as in smooth-invert chute flows (Eq. (6)), while Djenidi et al. (1999) observed self-preservation above d-type roughness. However the cavity recirculation and irregular fluid ejection processes interact with the boundary layer flow and contribute to some energy dissipation. In skimming flows, Chanson and Toombes (2001) expressed an analytical relationship between average cavity ejection frequency and flow resistance, while Lin and Rockwell (2001) showed that a higher order cavity flow frequency is related to the flow momentum thickness and velocity (Table 2). Djenidi et al. (1999) showed however that viscous drag is not negligible above d-type roughnesses.

7. Conclusion

Detailed air–water flow measurements were conducted in stepped open channels with flat horizontal steps (Fig. 1). The results show strong interactions between entrained air and turbulence.

Free-surface aeration (Figs. 3 and 4) is generated by high turbulence levels extending from the stepped invert up to the pseudo-free-surface (Fig. 6). The void fraction distributions were approximated by analytical solutions of the diffusion equation for air bubbles assuming non-constant diffusivity (Eqs. (2) and (3)). Air bubble and water droplet size measurements highlighted a broad range of detected particle sizes extending from less than 0.1 mm to over 20 mm (Fig. 8). The chord length distributions were skewed with preponderance of small particle sizes compared to the mean. In the bubbly flow region ($C < 0.3$) and in the spray region ($C > 0.7$), a cluster analysis showed a large number of particles (bubbles, droplets) travelling as part of clusters: e.g., about 30–45% of detected bubbles were parts of bubble clusters for $C < 0.3$. Most clusters comprised of two bubbles with no obvious preferential sizes (Fig. 9). It is suggested that bubble trapping in large-scale vortical structures is a dominant cluster mechanism for $C < 0.3$, but a different mechanism, possibly droplet ejection, takes place in the spray region.

For small water depths relative to the cavity roughness height (i.e. transition flows), air–water velocity profiles exhibited flat distributions at step edges (Fig. 5A). In skimming flows, the velocity distributions followed the same 1/6th power law (Fig. 5B) observed in smooth-invert chute flows. Measured turbulence levels were compared with water flow results on a stepped invert. The increase in turbulence levels was correlated to the number of entrained particles: $Tu \propto F^{1.5}$ (Eq. (7) and Fig. 7). That is, entrained air bubbles increase drastically turbulence levels across the entire mixture.

Overall strong interactions between entrained air bubbles and flow turbulence were observed, associated with large interfacial areas and high turbulence levels. For example, this mechanism contributes to substantial air–water mass transfer of atmospheric gases explaining re-oxygenation potential of stepped cascades, used for in-stream re-aeration and in treatment plants.

Acknowledgements

The first writer acknowledges the helpful discussion with Dr. J.L. Marie, Ecole Centrale de Lyon, France. The writers thank the reviewers for their critical and constructive comments.

Appendix A. Velocity measurements with dual-tip probes

With phase-detection intrusive probes, velocity measurement is based upon the successive detection of bubbles/droplets by two sensors (e.g. Fig. 2B). The technique assumes that the probe tips (or sensors) are aligned along a streamline, the slip velocity is small compared to the flow velocity, the bubble/droplet characteristics are little affected by the leading tip, and the bubble/droplet impact on the trailing tip is similar to that on the leading tip. In highly turbulent gas–liquid flows, the successive detection of a bubble by each probe tip is highly improbable, and it is common to use a cross-correlation technique (e.g. Fig. 2C). The shape of the cross-correlation function provides a further information on the turbulent velocity fluctuations (Kipphan, 1977; Chanson and Toombes, 2001). Flat cross-correlation functions are associated with large velocity fluctuations around the mean. Thin high cross-correlation curves are characteristics of small turbulent velocity fluctuations. The information must be corrected to account for the intrinsic noise of the leading probe signal and the turbulence intensity is related to the broadening of the cross-correlation function compared to the auto-correlation function.

The definition of the standard deviation of the velocity leads to

$$u'^2 = \frac{1}{N}\sum_{i=1}^{N}(v_i - V)^2 = \frac{V^2}{N}\sum_{i=1}^{N}\frac{1}{t_i^2}(t_i - T)^2 \tag{A.1}$$

where v_i is the instantaneous velocity data equal to $\Delta x/t_i$, t_i is the bubble travel time data, Δx is the distance between probe tips, V is the time-averaged velocity ($V = \Delta x/T$), N is the number of samples, and T is the travel time for which the cross-correlation function is maximum. With an infinitely large number of data points N, an extension of the mean value theorem for definite integrals may be used as the functions $1/t_i^2$ and $(t_i - T)^2$ are positive and continuous over the interval $[i = 1, N]$ (Spiegel, 1974). It implies that there exists at least one characteristic bubble travel time t' satisfying $t_1 \leqslant t' \leqslant t_N$ such that

$$\left(\frac{u'}{V}\right)^2 = \frac{1}{N}\frac{1}{t'^2}\sum_{i=1}^{N}(t - T)^2 = \frac{\sigma_t^2}{t'^2} \tag{A.2}$$

where σ_t is the standard deviation of the bubble travel time. That is, the standard deviation of the velocity is proportional to the standard deviation of the bubble travel time.

If the intrinsic noise of the probe signal is un-correlated with the turbulent velocity fluctuations with which the bubbles are advected, the standard deviation of the cross-correlation function σ_{xy} does satisfy:

$$\sigma_{xy}^2 = \sigma_{xx}^2 + \sigma_t^2 \tag{A.3}$$

where σ_{xx} is the standard deviation of the auto-correlation function (e.g. Harvey, 1993). Eq. (A.2) becomes

$$\frac{u'}{V} = \frac{\sqrt{\sigma_{xy}^2 - \sigma_{xx}^2}}{t'} \tag{A.4}$$

Assuming that $t' \sim T$ and that the bubble/droplet travel distance is a constant Δx, the turbulence intensity u'/V equals

$$\mathrm{Tu} = \frac{u'}{V} = \frac{\sqrt{\sigma_{xy}^2 - \sigma_{xx}^2}}{T} \tag{A.5}$$

Kipphan (1977) developed a slightly different reasoning for two-phase mixtures such as pneumatic conveying. He obtained

$$\frac{u'}{U_w} = \frac{\sqrt{\sigma_{xy}^2 - \sigma_{xx}^2}}{T} \tag{A.6}$$

where U_w is the time-averaged cross-section velocity.

A.1. Application

Experimental results obtained during the present study demonstrated that both cross-correlation and auto-correlation functions followed a Gaussian distribution (e.g. Fig. 2C). Assuming that the successive detections of bubbles by the probe sensors is a true random process, the cross-correlation function is a Gaussian distribution:

$$r(t) = r(T) \exp\left(-\frac{1}{2} \left(\frac{t - T}{\sigma_{xy}} \right)^2 \right) \tag{A.7}$$

where r is the cross-correlation function. Defining ΔT as a time scale satisfying: $r(T + \Delta T) = 0.5r(T)$, the standard deviation equals: $\sigma_{xy} = \Delta T/1.175$ for a true Gaussian distribution. Similarly the standard deviation of the auto-correlation function becomes: $\sigma_{xx} = \Delta t/1.175$ where Δt is the characteristic time for which the normalised auto-correlation function equals 0.5. Eq. (A.5) yields

$$\frac{u'}{V} = 0.851 \frac{\sqrt{\Delta T^2 - \Delta t^2}}{T} \tag{A.8}$$

A.2. Discussion

The derivation of both Eqs. (A.5) and (A.6) is based upon the assumption $t' \sim T$ which is made for all void fractions. For low void fractions, present results (Fig. 7) are close to the clear-water flow turbulence data obtained by Ohtsu and Yasuda (1997) for a similar flow configuration. The agreement between Eq. (A.5) and their data suggest that the assumption might be reasonable for low void fractions ($C < 0.05$) and low liquid fractions ($C > 0.95$). There is however no indication of its validity for $0.5 < C < 0.95$.

Appendix B. Void fraction distributions in self-aerated flows

In self-aerated open channel flows, the advective diffusion of air bubbles may be analytically predicted (Wood, 1984; Chanson, 1997a). At uniform equilibrium, the air concentration distribution is a constant with respect to the distance x in the flow direction and the continuity equation for air in the air–water flow yields

$$\frac{\partial}{\partial y}\left(D_t\frac{\partial C}{\partial y}\right)=\cos\alpha\frac{\partial}{\partial y}(u_r C) \tag{B.1}$$

where D_t is the turbulent diffusivity, u_r is the bubble rise velocity, α is the channel slope and y is measured perpendicular to the mean flow direction. The bubble rise velocity in a fluid of density $\rho_w(1-C)$ equals

$$u_r^2=[(u_r)_{Hyd}]^2(1-C) \tag{B.2}$$

where $(u_r)_{Hyd}$ is the rise velocity in hydrostatic pressure gradient (Chanson, 1997a). A first integration of the continuity equation for air in the equilibrium flow region leads to

$$\frac{\partial C}{\partial y'}=\frac{1}{D'}C\sqrt{1-C} \tag{B.3}$$

where $y'=y/Y_{90}$ and $D'=D_t/(u_r)_{Hyd}\cos\alpha Y_{90}$ is a dimensionless turbulent diffusivity. D' is the ratio of the air bubble diffusion coefficient to the rise velocity component normal to the flow direction times the characteristic transverse dimension of the shear flow. Assuming a homogeneous turbulence across the flow (i.e. D' constant), it yields

$$C=1-\tanh^2\left(K-\frac{y'}{2D'}\right) \tag{B.4}$$

where tanh is the hyperbolic tangent function and K a dimensionless integration constant (Chanson, 1997a).

Assuming that the dimensionless bubble diffusivity follows:

$$D'=\frac{C\sqrt{1-C}}{\lambda(K'-C)}$$

the integration of Eq. (B.3) yields

$$C=K'\left(1-\exp\left(-\lambda\frac{y}{Y_{90}}\right)\right) \tag{B.5}$$

where l and K' are dimensionless functions of the mean air content C_{mean} only (Chanson and Toombes, 2001). If the distribution of dimensionless bubble diffusivity D' follows:

$$D'=\frac{D_o}{1-2\left(\frac{y}{Y_{90}}-\frac{1}{3}\right)^2}$$

the solution of Eq. (B.3) is

$$C=1-\tanh^2\left(K''-\frac{\frac{y}{Y_{90}}}{2D_o}+\frac{\left(\frac{y}{Y_{90}}-\frac{1}{3}\right)^3}{3D_o}\right) \tag{3}$$

where K'' and D_o are functions of the mean void fraction only.

B.1. Remarks

Although Eq. (B.1) assumes uniform equilibrium flow conditions, several researchers showed that its analytical solutions are applicable in gradually varied flows above smooth chutes (Wood, 1984; Chanson, 1997a,b) and stepped chutes (Matos, 2000; Chanson and Toombes, 2001).

References

Ackers, P., White, W.R., Perkins, J.A., Harrison, A.J.M., 1978. Weirs and Flumes for Flow Measurement. John Wiley, Chichester, UK, 327 pp.

Boes, R.M., 2000. Zweiphasenstroömung und Energieumsetzung an Grosskaskaden. (Two-phase flow and energy dissipation on cascades.) Ph.D. Thesis, VAW-ETH, Zürich, Switzerland (in German) (also Mitteilungen der Versuchsanstalt fur Wasserbau, Hydrologie und Glaziologie, ETH-Zurich, Switzerland, No. 166).

Bos, M.G., 1976. Discharge Measurement Structures. Publication No. 161, Delft Hydraulic Laboratory, Delft, The Netherlands (also Publication No. 20, ILRI, Wageningen, The Netherlands).

Cain, P., 1978. Measurements within self-aerated flow on a large spillway. Ph.D. Thesis, Refs. 78–18, Department of Civil Engineering, University of Canterbury, Christchurch, New Zealand.

Chamani, M.R., Rajaratnam, N., 1994. Jet flow on stepped spillways. J. Hydraul. Eng., ASCE 120, 254–259.

Chamani, M.R., Rajaratnam, N., 1999. Characteristics of skimming flow over stepped spillways. J. Hydraul. Eng., ASCE 125, 361–368, Discussion: 126, 860–872. Closure: 126, 872–873.

Chanson, H., 1993. Self-aerated flows on chutes and spillways. J. Hydraul. Eng., ASCE 119, 220–243, Discussion: 120, 778–782.

Chanson, H., 1994. Hydraulics of nappe flow regime above stepped chutes and spillways. Aust. Civil Eng. Trans., I.E. Aust. CE36, 69–76.

Chanson, H., 1995. Hydraulic Design of Stepped Cascades, Channels, Weirs and Spillways. Pergamon, Oxford, UK, 292 pp.

Chanson, H., 1997a. Air Bubble Entrainment in Free-surface Turbulent Shear Flows. Academic Press, London, UK.

Chanson, H., 1997b. Air bubble entrainment in open channels. Flow structure and bubble size distributions. Int. J. Multiphase Flow 23, 193–203.

Chanson, H., 2001. The Hydraulics of Stepped Chutes and Spillways. Swets & Zeitlinger, Lisse, The Netherlands.

Chanson, H., Brattberg, T., 1998. Air entrainment by two-dimensional plunging jets: the impingement region and the very-near flow field. In: Proceedings of the 1998 ASME Fluids Engineering Conference, FEDSM'98, Washington DC, USA, June 21–25, Paper FEDSM98-4806, 8 p (CD-ROM).

Chanson, H., Brattberg, T., 2000. Experimental study of the air-water shear flow in a hydraulic jump. Int. J. Multiphase Flow 26, 583–607.

Chanson, H., Toombes, L., 1997. Flow aeration at stepped cascades. Research Report No. CE155, Department of Civil Engineering, University of Queensland, Australia, 110 pp.

Chanson, H., Toombes, L., 2000. Stream reaeration in nonuniform flow: macroroughness enhancement. J. Hydraul. Eng., ASCE 126, 222–224, Discussion.

Chanson, H., Toombes, L., 2001. Experimental investigations of air entrainment in transition and skimming flows down a stepped chute. Application to embankment overflow stepped spillways. Research Report No. CE158, Department of Civil Engineering, The University of Queensland, Brisbane, Australia, 74 pp.

Chanson, H., Yasuda, Y., Ohtsu, I., 2000. Flow resistance in skimming flow: a critical review. In: Minor, H.E., Hager, W.H. (Eds.), International Workshop on Hydraulics of Stepped Spillways, Zürich, Switzerland. Balkema Publ, pp. 95–102.

Comolet, R., 1979. Vitesse d'ascension d'une bulle de gaz isolée dans un liquide peu visqueux. (The Terminal Velocity of a Gas Bubble in a Liquid of Very Low Viscosity.) J Mécan. Appl. 3, 145–171 (in French).

Crowe, C., Sommerfield, M., Tsuji, Y., 1998. Multiphase Flows with Droplets and Particles. CRC Press, Boca Raton, USA, 471 pp.

Cummings, P.D., Chanson, H., 1999. An experimental study of individual air bubble entrainment at a planar plunging jet. Chem. Eng. Res. Des., Trans. IChemE, Part A 77 (A2), 159–164.

Djenidi, L., Anselmet, F., Antonia, R.A., 1994. LDA measurements in a turbulent boundary layer over a D-type rough wall. Exp. Fluids 16, 323–329.

Djenidi, L., Elavarasan, R., Antonia, R.A., 1999. The turbulent boundary layer over transverse square cavities. J. Fluid Mech. 395, 271–294.

Elavarasan, R., Pearson, B.R., Antonia, R.E., 1995. Visualization of near wall region in a turbulent boundary layer over transverse square cavities with different spacing. In: Proceedings of the 12th Australasian Fluid Mechanics Conference, AFMC, Sydney, Australia, vol. 1, pp. 485–488.

Ervine, D.A., Falvey, H.T., 1987. Behaviour of turbulent water jets in the atmosphere and in plunge pools. In: Proceedings of the Institution of Civil Engineering, London, Part 2, March 1987, 83, pp. 295–314. Discussion: Part 2, March–June 1988, 85, pp. 359–363.

Harvey, A.C., 1993. Time Series Models. Harvester Wheatsheaf, London.

Haugen, H.L., Dhanak, A.M., 1966. Momentum transfer in turbulent separated flow past a rectangular cavity. J. Appl. Mech., Trans. ASME September, 464–641.

Hoyt, J.W., Taylor, J.J., 1977. Waves on water jets. J. Fluid Mech. 83, 119–127.

Keulegan, G.H., Patterson, G.W., 1940. A criterion for instability of flow in steep channels. Trans. Am. Geophys. Union, Pt II 21, 594–596.

Kipphan, H., 1977. Bestimmung von Transportkenngrößen bei Mehrphasenströmungen mit Hilfe der Korrelationsmeßtechnik. Chem. Ingenieur Tech. 49, 695–707.

Lance, M., Bataille, J., 1991. Turbulence in the liquid phase of a uniform bubbly air–water flow. J. Fluid Mech. 222, 95–118.

Lin, J.C., Rockwell, D., 2001. Organized oscillations of initially turbulent flow past a cavity. AIAA J. 39, 1139–1151.

Liu, T.J., Bankoff, S.G., 1993. Structure of air–water bubbly flow in a vertical pipe—II. Void fraction, bubble velocity and bubble size distribution. Int. J. Heat Mass Transfer 36, 1061–1072.

Matos, J., 2000. Hydraulic design of stepped spillways over RCC dams. In: Minor, H.E., Hager, W.H. (Eds.), International Workshop on Hydraulics of Stepped Spillways, Zürich, Switzerland. Balkema Publ, pp. 187–194.

Matos, J., Yasuda, Y., Chanson, H., 2001. Interaction between free-surface aeration and cavity recirculation in skimming flows down stepped chutes. In: Proceedings of the 29th IAHR Congress, Beijing, China, Theme D, Subtheme D5-24 (CD-ROM).

Mudde, R.F., Saito, T., 2001. Hydrodynamical similarities between bubble column and bubbly pipe flow. J. Fluid Mech. 437, 203–228.

Ohtsu, I., Yasuda, Y., 1997. Characteristics of flow conditions on stepped channels. In: Proceedings of the 27th IAHR Biennal Congress, San Francisco, USA, Theme D, pp. 583–588.

Ohtsu, I., Yasuda, Y., Takahashi, M., 2000. Characteristics of skimming flow over stepped spillways. J. Hydraul. Eng., ASCE 126, 869–871 (Discussion).

Rajaratnam, N., 1990. Skimming flow in stepped spillways. J. Hydraul. Eng., ASCE 116, 587–591, Discussion: 118, 111–114.

Rein, M., 1998. Turbulent open-channel flows: drop-generation and self-aeration. J. Hydraul. Eng., ASCE 124 (1), 98–102, Discussion: 125, 668–670.

Schlichting, H., 1979. Boundary Layer Theory, seventh ed. McGraw-Hill, New York, USA.

Spiegel, M.R., 1974. Mathematical Handbook of Formulas and Tables. McGraw-Hill Inc., New York, USA.

Sumer, B.M., Cokgor, S., Fredsøe, J., 2001. Suction Removal of Sediment from between Armor Blocks. J. Hydraul. Eng., ASCE 127, 293–306.

Tantirige, S.C., Iribarne, A.P., Ojhas, M., Trass, O., 1994. The turbulent boundary layer over single V-shaped cavities. Int. J. Heat Mass Transfer 37, 2261–2271.

Tooby, P.F., Wick, G.L., Isacs, J.D., 1977. The motion of a small sphere in a rotating velocity field: a possible mechanism for suspending particles in turbulence. J. Geophys. Res. 82, 2096–2100.

Toombes, L., 2002. Experimental study of air–water flow properties on low-gradient stepped cascades. Ph.D. Thesis, Department of Civil Engineering, University of Queensland, Brisbane, Australia.

Toombes, L., Chanson, H., 2000. Air–water flow and gas transfer at aeration cascades: a comparative study of smooth and stepped chutes. In: Minor, H.E., Hager, W.H. (Eds.), International Workshop on Hydraulics of Stepped Spillways, Zürich, Switzerland. Balkema Publ, pp. 77–84.

Tozzi, M., Taniguchi, E., Ota, J., 1998. Air concentration in flows over stepped spillways. In: Proceedings of the 1998 ASME Fluids Engineering Conference, FEDSM'98, Washington DC, USA, June 21–25, Paper FEDSM98-5053, 7 pp.

Wang, S.K., Lee, S.J., Jones, O.C., Lahey, R.T., 1990. Statistical analysis of turbulent two-phase pipe flow. J. Fluids Eng., ASME 112 (March), 89–95.

Wood, I.R., 1984. Air entrainment in high speed flows. In: Kobus, H. (Ed.), Proceedings of the International Symposium on Scale Effects in Modelling Hydraulic Structures, IAHR, Esslingen, Germany, paper 4.1.

Wood, I.R., 1991. Air entrainment in free-surface flows. In: IAHR Hydraulic Structures Design Manual No. 4, Hydraulic Design Considerations. Balkema Publ, Rotterdam, The Netherlands, 149 pp.